Application of digital image processing in slope surface runoff velocity analysis under simulated rainfall conditions

Tiexiong Gong and Yuanjun Zhu

ABSTRACT

To have accurate runoff velocity, there is need to improve dye tracer method for estimating surface runoff velocity. This can enhance the calculations of relevant hydrologic parameters that will lead to a better understanding of hydrological processes and soil erosion. In this study, an integrated dye tracer and image processing method (*IPV*) and dye tracer method (*AOV*), respectively, were used to estimate runoff velocity under three slope gradients (5°, 10°, and 15°) and three slope positions (up-slope, mid-slope, and down-slope). The results showed more variation in runoff velocity under *IPV* than *AOV*. Both *IPV* and *AOV* were positively correlated with slope gradient. *IPV* values were close to *AOV* ones for slope gradients $\leq 5°$, but were significantly different for slope gradients $\geq 10°$. The mean *AOV* value was 10.6% higher than that of *IPV*. Regression analysis showed that compared with *AOV*, *IPV* overestimated and underestimated runoff under low and high runoff velocity conditions, respectively. The use of image processing in *IPV* was advantageous because of its ease of use with fewer artificial errors and its suitability for lateral diffusion of runoff. Irrespectively, additional studies are needed to verify and/or improve further the use of this method in runoff velocity analysis.

Key words | dye tracer, image processing, runoff velocity, simulated rainfall, slope gradient

Tiexiong Gong
Yuanjun Zhu (corresponding author)
State Key Laboratory of Soil Erosion and Dryland Farming on the Loess Plateau,
Northwest A&F University,
Yangling 712100,
China;
Institute of Soil and Water Conservation,
Chinese Academy of Sciences and Ministry of Water Resources,
Yangling 712100,
China;
and
University of Chinese Academy of Sciences,
Beijing 100049,
China
E-mail: *zhuyuanjun@foxmail.com*

INTRODUCTION

Surface runoff velocity is a key hydrologic parameter in slope hydrological processes and soil erosion. First, it directly affects sediment yield by controlling the partitioning of rainfall into runoff and infiltration (Zhang *et al.* 2003, 2016; Chen *et al.* 2008; Lei *et al.* 2010; Meral 2016). An accurate estimation of surface runoff velocity is needed for a reliable determination of runoff coefficient and sediment yield (Del Giudice *et al.* 2014; Zhang *et al.* 2014). Second, surface runoff velocity is used to derive hydrologic parameters such as Reynolds number and Manning coefficient used to determine slope flow regimes, slope hydrologic processes, and erosion–sediment relationships (Philip 1954; Bissonnais & Singer 1992; Fohrer *et al.* 1999; Furumai *et al.* 2005; Ares *et al.* 2016; Sun *et al.* 2016). Finally, surface runoff velocity dominates runoff kinetic energy. The accurate estimation of runoff velocity can benefit the calculation of runoff kinetic energy, which can be used to predict sediment carrying capacity and sediment yield (Wilson 1973; Williams & Berndt 1977; Abrahams *et al.* 1986; Li *et al.* 1996; Nadal-Romero *et al.* 2013; Rahma *et al.* 2013; Shi *et al.* 2013, 2014; Yan *et al.* 2013). Hence, the estimation of runoff velocity is critical in soil science and hydrology.

Different technologies and methods have been developed in the past decades to estimate runoff velocity, among which tracer methods are the most popular. Tracers vary from dye (Abrahams *et al.* 1986; Zhang *et al.* 2010) to electrolyte pulse (Planchon *et al.* 2005; Lei *et al.* 2010), large and light weight particles (Singh *et al.* 1995, 2005; Tauro *et al.* 2012a, 2012b; Muste *et al.* 2014), thermal (de Lima & Abrantes 2014; de Lima *et al.* 2015), magnetic

doi: 10.2166/nh.2017.040

(Ventura *et al.* 2001) and heat (Angermann *et al.* 2012) pulses, liquid water isotope (Berman *et al.* 2009), and radioisotope (Gardner & Dunn 1964). Of all these, dye tracer is the earliest used tracer, and it is still widely used in laboratory experiments due to its ease of operation and stability. Electrolyte tracers measure changes in runoff solute concentration that is inverted for runoff velocity. This method is based on mathematical solutions to solute transport in shallow runoff conditions (Lei *et al.* 2010). Moreover, it is easily affected by sediment charge, resulting in poor correlation between runoff velocity and dispersion coefficient. Using a large and light weight particle tracer like sawdust (diameter < 1 mm) to estimate runoff velocity is another option. Sawdust needs image velocimetry that is composed of a high-speed digital camera to record its movement (Muste *et al.* 2014). On the one hand, sawdust could also affect the surface runoff flow regime and, on the other hand, sediment load can change sawdust movement. Both of them can reduce the reliability of runoff velocity estimation by this method. An ingenious alternative method is the use of fluorescent particle tracer to estimate overland flow velocity (Tauro *et al.* 2012a, 2012b). Although this method reduces the effects of sediment concentration on runoff velocity measurement, it requires complex devices for fluorography. Thermal tracer technique uses infrared thermography to visualize very shallow flows and allows quantitative measurement of overland and rill flow velocities by injecting a heated dye (Schuetz *et al.* 2012; de Lima & Abrantes 2014). While injecting high temperature water into runoff is difficult to operate in most rainfall experiments, other tracers like liquid water isotope and radioisotope are expensive and complicated, equipment-dependent and therefore hard to apply in laboratory and field experiments.

The traditional dye tracer method used to determine surface runoff velocity is done by adding dye to runoff and measuring the time the dyed runoff takes to move over a given distance on a slope. The accuracy of the estimated runoff velocity depends on the selection of calibration coefficient in the velocity calculation, which is closely related to the flow regime (Horton *et al.* 1934; Emmett 1970; Foster *et al.* 1984; King & Norton 1992; Luk & Merz 1992). Furthermore, it often induces artificial error when determining the time the dyed runoff flows over a given distance (Luk & Merz 1992; Abrahams & Atkinson 1993). It is also time- and labor-consuming. Currently, high-resolution digital cameras are increasingly used to capture changes on slope surfaces for soil and water processes. Digital cameras only record change in velocity at any time period, but also clearly identify dyed runoff front. Therefore, the use of integrated dye tracer and image processing to estimate slope runoff velocity could reduce artificial error and increase the accuracy of estimation of surface runoff velocity. However, the accuracy and reliability of this method need to be improved by conducting further laboratory experiments.

In this study, rainfall simulation was used to generate runoff on various slope gradients and the runoff periodically dyed to measure runoff velocity by dye tracer method. A digital camera was next used to record the progress of the dyed runoff flow on the slopes. Then we used image processing software to extract images from the recorded video by the camera and to detect the distance that the dyed runoff moved over a given time to calculate runoff velocity. The aim of the study was to: (1) demonstrate the process of runoff velocity estimation using the integrated dye tracer and image processing method; (2) compare the measured velocity under the method with that under only the dye tracer method; and (3) explain the differences between the two methods.

MATERIALS AND METHODS

Materials

The runoff simulation experiment was carried out in a rainfall simulation hall belonging to the State Key Laboratory of Soil Erosion and Dryland Farming on the Loess Plateau. A metal box (3 m long, 1 m wide, and 0.35 m deep) filled with soil was used for the slope runoff simulation. Soil sieved through a 5 mm mesh and air-dried was loaded in the metal box to the depth of 0.3 m and the soil maintained at a bulk density of 1,300 $kg \cdot m^{-3}$. The soil was collected from a local field surface soil (0–0.2 m) with a particle composition of 33.6% clay, 39.7% silt, and 26.7% sand, respectively. A digital camera (Sony DSC x-1) was set at a height of 3 m above the ground and 3 m away from the front wall of the metal box (Figure 1(a)). There were three slope gradients (5°, 10°, and 15°) in the rainfall simulation

experiment. The general specifications of the digital camera are shown in Table 1. The rainfall intensity was 60 mm·h^{-1} and each rainfall event lasted for 60 min with a uniform coefficient of 0.9. The dye was potassium permanganate solution with a purple color. The reason for using potassium permanganate solution was that it can dye runoff immediately after application and can last for a long time. Also, the color of potassium permanganate was different from

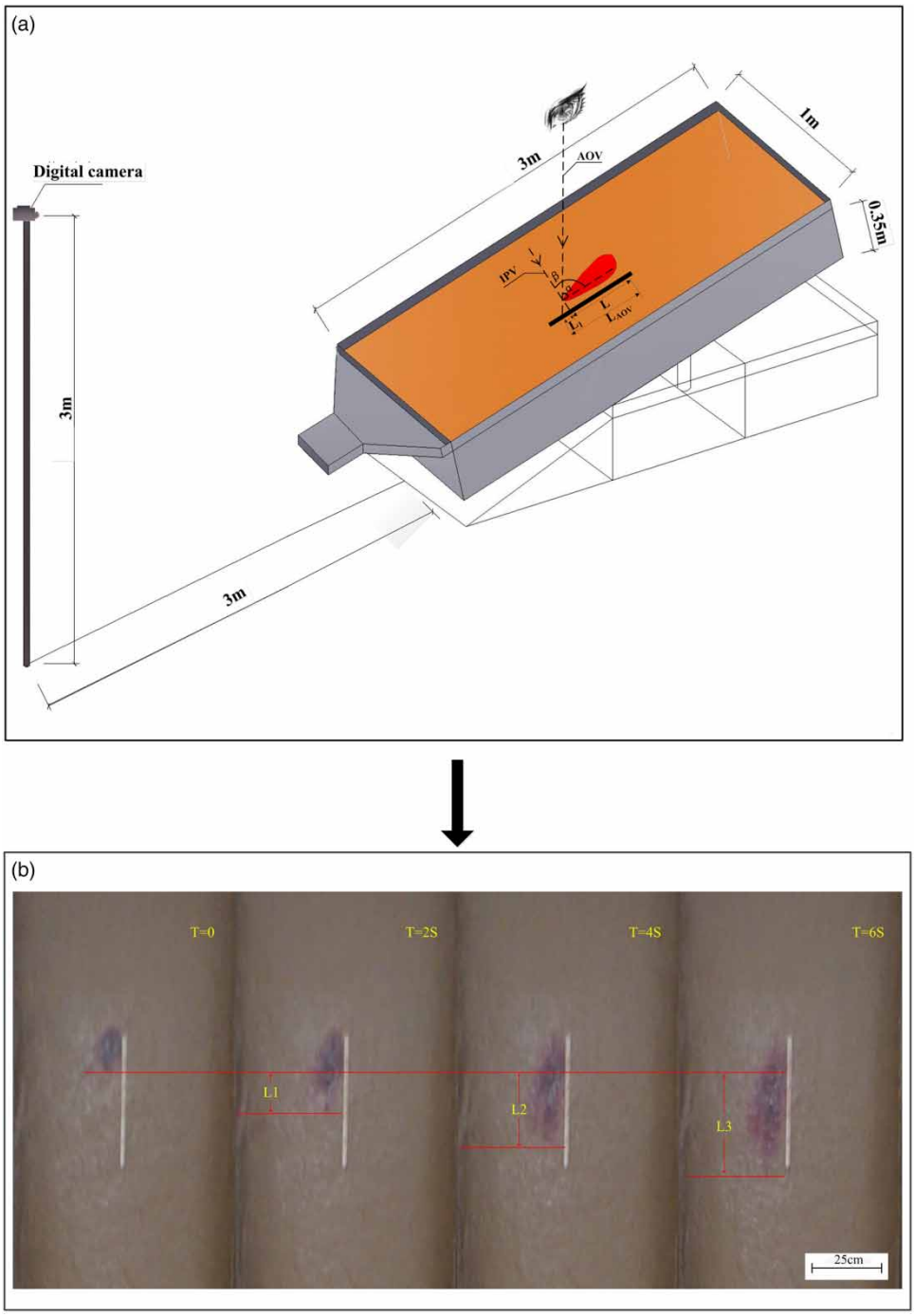

Figure 1 | A schematic for the experiment (a) and the determination of runoff velocity under the integrated dye tracer and image processing method (b).

Table 1 | General specifications of the digital camera used in the study

Item	Unit	Specification
Optical resolution	Pixel	1,920 × 1,080
CMOS size	Inch	1/3
Focal length	cm	~25 cm – ∞
Field of view	°	120
Recording speed	Frame per second	30

that of the soil and was easily detectable during image processing.

Methods

After the runoff had been generated for 5 min, the dye was added every 5 min into the runoff at three slope positions: up-slope (0–1 m), mid-slope (1–2 m), and down-slope (2–3 m) along the top–bottom direction. Two methods (dye tracer, and integrated dye tracer and image processing) were used to estimate surface runoff velocity under the three slope gradients. Runoff velocity determined by the dye tracer method was denoted as *AOV* and the one determined by the integrated dye tracer and image processing method denoted as *IPV*.

Dye tracer method

During the simulated rainfall, a 0.5 m long ruler was placed horizontally on the soil surface. When the generated runoff velocity on the slope was steady, the dye was added to the runoff and a stopwatch used to record the time (T) that the dyed runoff flowed over the length (L) of the ruler. *AOV* was then calculated as:

$$AOV = k \cdot \frac{L}{T} \tag{1}$$

where k is the calibration coefficient of runoff velocity; T is the time that the dyed runoff flowed over the length of the ruler (s); and L is the ruler length (m).

Numerous studies suggest that the coefficient k varies with flow regime. Based on theoretical analysis, Horton *et al.* (1934) recommended a calibration coefficient of 0.65 for laminar flow. Emmett (1970) suggested different coefficient ranges, which vary from 0.5–0.6 for laminar flow, to 0.8 for transient flow under laboratory conditions, and to 0.45–0.50 under field conditions. Other studies have set the coefficient at 0.52 for laminar flow and 0.75 for transient and turbulent flows (Luk & Merz 1992). The calibration coefficient k was set at 0.65 in this study – a trade-off value for slope length and flow regime (Li *et al.* 1996; Dunkerley 2001; Zhang *et al.* 2010).

Integrated dye tracer and image processing method

The *IPV* procedure was as follows: image acquisition → image rectification and background calibration → runoff velocity measurement. First, we used the digital camera to record the whole runoff simulation process. Then, slope surface images containing information on dyed runoff flow on the slope were extracted from the runoff simulation video at an interval of 2 s using ImageJ software (version: 1.43, developed by National Institute of Health). Second, the projection transformation of the extracted images was taken (generating orthoimages of the slope surface) and background calibration (making the dyed runoff easily distinguishable from soil and non-dyed runoff for runoff front detection) using Photoshop software (version: 15.0) for the next image processing. After that, every four frame sequential images were montaged as one image for *IPV* calculation in Image-Pro Plus software (version: 5.0).

In this study, three distances through which the dyed runoff flowed on the slope (denoted as L_1, L_2, and L_3) were detected by image processing (Figure 1(b)). Then, the runoff velocity was calculated as follows:

$$V_1 = \frac{L_1}{T}, V_2 = \frac{L_2}{2 \cdot T}, V_1 = \frac{L_3}{3 \cdot T} \tag{2}$$

where L_1, L_2, and L_3 are the distances through which runoff flows during the three periods (m); V_1, V_2, and V_3 are the velocities for runoff flow over the distances L_1, L_2, and L_3, respectively ($m \cdot s^{-1}$); and T is the time interval at which the images were extracted from the video (s).

The equation for the calculation of *IPV* is expressed as:

$$IPV = \frac{V_1 + V_2 + V_3}{3} \tag{3}$$

where *IPV* is runoff velocity determined by the integrated dye tracer and image processing method ($m \cdot s^{-1}$).

RESULTS

Runoff velocity change during rainfall

The changes in *AOV* and *IPV* during rainfall on the three slope gradients are shown in Figure 2. Generally, the trends in both *AOV* and *IPV* increased from the start to the end of the rainfall event. Also, both *AOV* and *IPV* had the same trend, in that runoff velocity increased with increasing slope gradient. In other words, the values for *AOV* and *IPV* were higher under 15° than under 10° slope gradient, which in turn was higher than under 5° slope gradient (the lowest). This result indicated that *IPV* (determined by the integrated dye tracer and image processing method) captured the relationship connecting runoff velocity, rainfall duration, and slope gradient. However, there were differences in the degree of fluctuation of runoff velocity between *AOV* and *IPV* during a rainfall event, with a higher degree of fluctuation in *IPV* than *AOV*-generated runoff velocity.

The average values of *AOV* and *IPV*-generated runoff velocity under three different slope gradients are plotted in Figure 3. When the slope gradient = 5°, the average value of *AOV*-generated runoff velocity was close to that of *IPV* and there was no significant difference between the two methods. When the slope gradient increased to 10° and to 15°, there were significant differences between average *AOV*-generated runoff velocity and *IPV* ($p < 0.05$). The average value of *AOV*-generated runoff velocity was higher than that of *IPV* under 10° and 15° slope gradients. Compared with that under 15° slope gradient, the average values of *IPV*-generated runoff velocity decreased by 14% and 26%, respectively, under 10° and 15° slope gradients.

Runoff velocity change with slope position

We also calculated *AOV* and *IPV*-generated runoff velocities at the three slope positions – up-slope, mid-slope, and down-slope. Figure 4 shows the changes in *AOV* and *IPV*-generated runoff velocities. The average value of *AOV*-generated runoff velocity showed an increasing trend from the up-slope to down-slope under the three slope gradients. However, the average value of *IPV*-generated runoff velocity at the three slope gradients was different from that under *AOV*-generated runoff velocity. When the slope gradient = 5°, average *IPV* had little variation along the slope. But when the slope gradient = 10°, average *IPV* increased largely from up-slope to mid-slope, and then decreased slightly at down-slope. As the slope gradient = 15°, average *IPV* increased from up-slope to down-slope, but the range of change under *IPV* was smaller than that under *AOV*.

Runoff velocity comparison

We compared runoff velocities determined by the *AOV* and *IPV* methods. It showed that both *AOV* and *IPV* were not well distributed along the 1:1 line (dotted line in Figure 5), suggesting that differences existed in runoff velocity

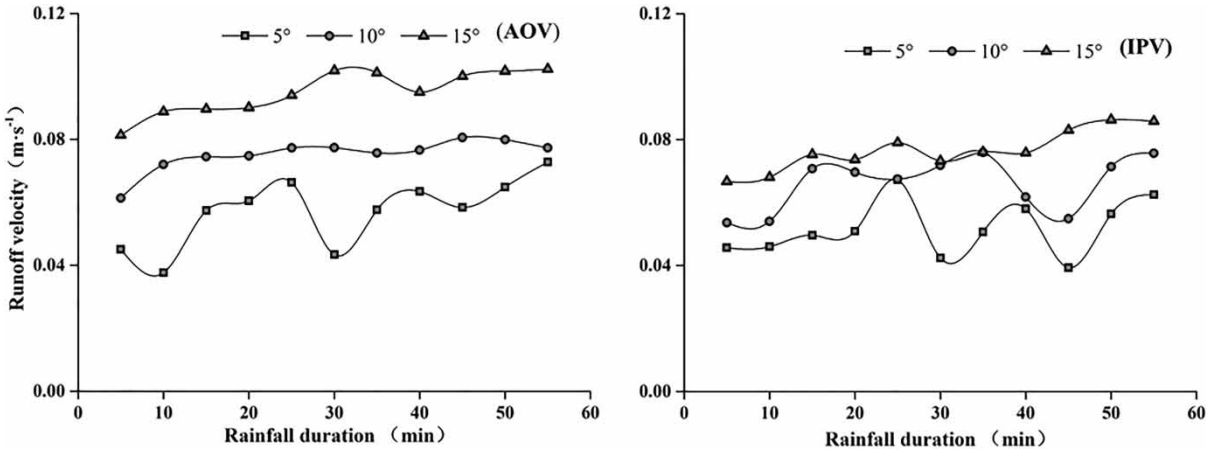

Figure 2 | Changes in *AOV* and *IPV*-generated runoff velocity during a rainfall event on three different slope gradients.

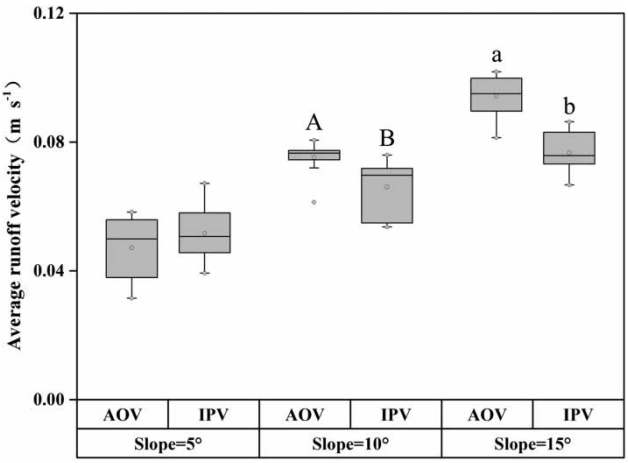

Figure 3 | Average values of *AOV* and *IPV*-generated runoff velocities under three different slope gradients. The signs above the box denote significance level.

estimation by the two methods. More specifically, when slope gradient = 5°, *IPV*-generated runoff velocities were higher than that of *AOV* (for which runoff velocity was at the lowest level). As runoff velocity increased under the different slope gradients, the average for *IPV* became close to that for *AOV*, but with larger variation under *IPV*. When slope gradients = 10° and 15°, *IPV* was basically distributed below the 1:1 line. This suggested that runoff velocity was underestimated by the integrated dye tracer and image processing method. Under the two slope gradients, the variation in *IPV* was still larger than that in *AOV*. A linear fit of *IPV* and *AOV* showed that the fitted slope equations for all the three slope gradients were less than 1.

DISCUSSION

For a long time, the estimation of runoff velocity has focused mainly on hydrological processes of slopes. Irrespectively, runoff velocity estimation is still a tedious challenge because of its dependence on so many variables, including observer trait, observation position, sediment load, rainfall event, and slope gradient (Dunne *et al.* 1991; Fox & Bryan 2000; Chaplot & Le Bissonnais 2003; Assouline & Ben-Hur 2006; Fang *et al.* 2015; Shen *et al.* 2016). In this study, we integrated dye tracer and image processing and used it for runoff velocity measurement. The results showed that the change trends in runoff velocity determined by the *IPV* method (the integrated method) were similar to that determined by the *AOV* method (dye tracer method) under three slope gradients. However, some differences were noted between the *IPV* and *AOV* methods. The results suggested that compared with *AOV*, *IPV* overestimated runoff velocity under low runoff conditions, but underestimated it under high runoff conditions. This was mainly attributed to three factors:

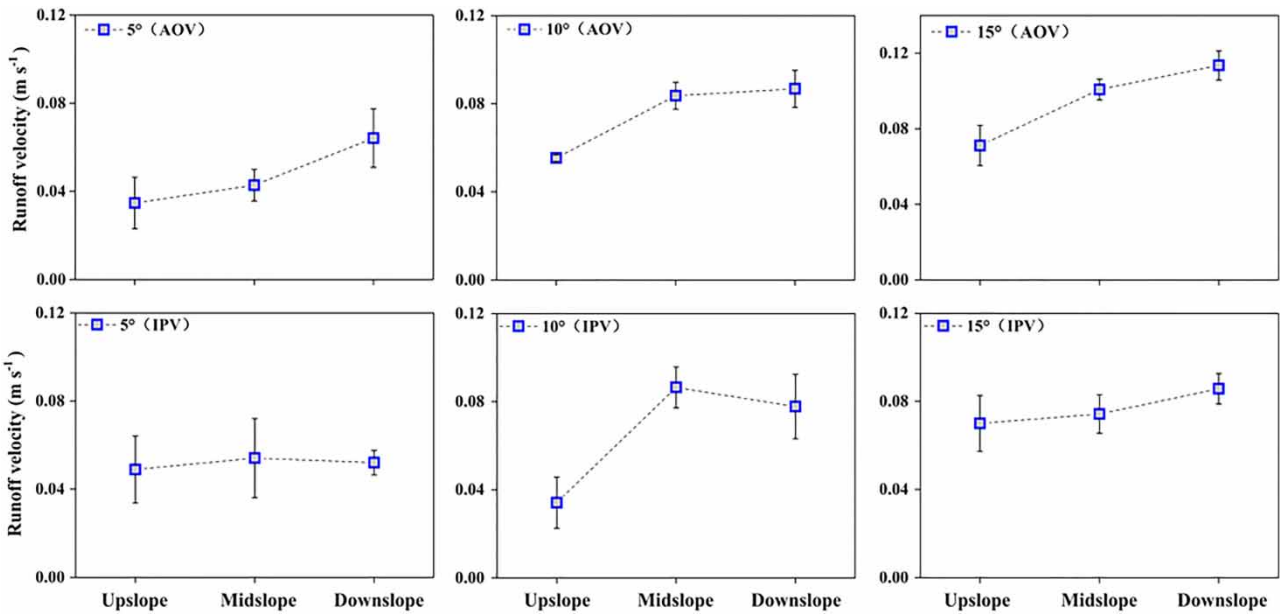

Figure 4 | Changes in *AOV* and *IPV*-generated runoff velocities at three different slope positions under three different slope gradients.

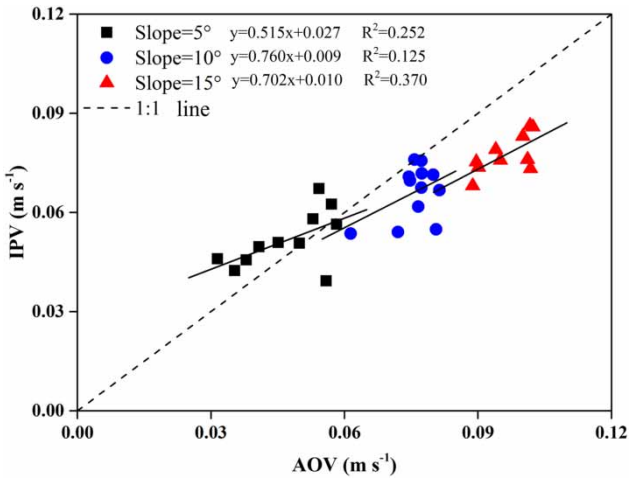

Figure 5 | Plot of *AOV*-generated runoff velocity against *IPV*-generated runoff velocity on different slope gradients under the same rainfall event.

(1) the position of the observer, (2) the pattern of the ruler on the slope, and (3) the observer judgment of dyed runoff front. For the dye tracer method (*AOV*), the distance the dyed runoff travels is the length of the ruler. The observer position and ruler pattern on the slope can cause an under-shooting of distance compared with the actual ruler length (Xia *et al.* 2007). For instance, when the observer stands above the vertical extension cord of the ruler bottom endpoint, the angle between the observer's eye and the ruler endpoint is less than 90° (Figure 1(a)). Then, the distance that the dyed runoff travels is shorter than the ruler length, but the observer reads it as the ruler length, and this results in a shorter time than the actual time the dyed runoff travels through the ruler length. Based on the runoff velocity equation (distance/time), time decreases as velocity increases.

In this study, the observer stood at the upper part of the ruler in order to facilitate dyeing of the runoff, resulting in the error conditions explained above and further causing *AOV* to be larger than *IPV*. The pattern of the ruler on the slope affected the estimation of runoff velocity. In theory, the ruler is placed vertically to the wall of the soil box in order to make the ruler length equal to the travel distance of the dyed runoff front. When the ruler is not vertical, the length can mistakenly be read as the travel distance of the dyed runoff front under artificial observation, whereas such error does not occur under image processing. In human observation, the distance that the dyed runoff moves is the length of the ruler (L), whereas the distance in image processing (L_i) is equal to the cosine of L ($L_i = L \times \cos(\alpha)$) (Figure 1). This results in higher *AOV* than *IPV*. In the integrated method, the obstacles highlighted above are completely avoided. As dyed runoff front is difficult to determine, researchers often resort to the use of human observation, which gives uncertain travel distances (Xia *et al.* 2007). It is therefore clear that *AOV* is, to some extent, uncertain and largely dependent on experience. Conversely, the image processing analyzes color changes that can be used to determine runoff front. Theoretically, this method is far more reliable.

Finally, the calibration coefficient (set at 0.65 in this study) is an empirical number in the dye tracer method that is dependent on flow regime. Several studies recommend a smaller calibration coefficient than the one used in this study (Luk & Merz 1992; Abrahams & Atkinson 1993; Berger *et al.* 2010; Fang *et al.* 2015). Thus, the calibration coefficient can also be a factor for the higher *AOV* than *IPV*; while in the method of integrating the dye tracer and image processing, we do not need this coefficient. Hence, it is an advantage over the traditional dye tracer method. At the same time, this method could be used for calculating or validating the coefficient used in the traditional dye tracer method.

In general, the reasons for the discrepancies between *AOV* and *IPV* could be a lot more complex than the explanations given above. However, the integrated method (dye tracer and image processing) used in this study has strong advantages over the traditional dye tracer method. The integration of dye tracer and image processing avoids the obstacles related to observer trait, observation position, and precision runoff front determination. Above all, the integrated method can calculate lateral runoff diffusion, which is not possible with the traditional dye tracer method. Irrespectively, there is the need to build sufficient data on this method in order to more fully understand its range of strength and weakness.

CONCLUSIONS

A method of integrating dye tracer and image processing was developed (*IPV*) and used to calculate slope runoff velocity, which was then compared with that of the traditional dye tracer method (*AOV*). The results showed that the

integrated method captured well the changes in runoff velocity for the simulated rainfall event. The estimated runoff velocity by the integrated method was positively related to slope gradient. The average velocity under *IPV* was close to that under *AOV* for the 5° slope gradient, but was significantly different for the 10° and 15° slope gradients. The mean velocity for the *AOV* method was 10.6% higher than that of the *IPV* method. Compared with the dye tracer (*AOV*) method, the integrated (*IPV*) method overestimated runoff velocity under low runoff velocity condition and underestimated it under high runoff velocity condition. The image processing technique used in runoff velocity estimation showed uncertainties in runoff velocity estimation under the traditional dye tracer method and in the selection of calibration coefficient based on flow regime. On the other hand, the integrated dye tracer and image processing method still needs further improvement through rigorous experimentation to ensure higher accuracy and wider application.

ACKNOWLEDGEMENTS

This work was financially supported by the National Natural Science Foundation of China (41371242, 41530854, and 41571130081) and the Key Research Program of the Chinese Academy of Sciences (KFZD-SW-306). We thank the State Key Laboratory of Dryland Farming and Soil Erosion on the Loess Plateau for providing the requirements for the experiment. Special thanks go to the editors and reviewers for the exciting input during the review phase of the paper.

REFERENCES

Abrahams, A. D. & Atkinson, J. F. 1993 Relation between grain velocity and sediment concentration in overland flow. *Water Resour. Res.* **29** (9), 3021–3028.

Abrahams, A. D., Parsons, A. J. & Luk, S. H. 1986 Field measurement of the velocity of overland flow using dye tracing. *Earth Surf. Processes Landforms* **11** (6), 653–657.

Angermann, L., Krause, S. & Lewandowski, J. 2012 Application of heat pulse injections for investigating shallow hyporheic flow in a lowland river. *Water Resour. Res.* **48** (12), W00P02.

Ares, M. G., Bongiorno, F., Holzman, M., Chagas, C., Varni, M. & Entraigas, I. 2016 Water erosion and connectivity analysis during a year with high precipitations in a watershed of Argentina. *Hydrol. Res.* **47** (6), 1239–1252.

Assouline, S. & Ben-Hur, M. 2006 Effects of rainfall intensity and slope gradient on the dynamics of interrill erosion during soil surface sealing. *Catena* **66** (3), 211–220.

Berger, C., Schulze, M., Rieke-Zapp, D. & Schlunegger, F. 2010 Rill development and soil erosion: a laboratory study of slope and rainfall intensity. *Earth Surf. Processes Landforms* **35** (12), 1456–1467.

Berman, E. S., Gupta, M., Gabrielli, C., Garland, T. & McDonnell, J. J. 2009 High-frequency field-deployable isotope analyzer for hydrological applications. *Water Resour. Res.* **45** (10), W10201.

Bissonnais, Y. L. & Singer, M. J. 1992 Crusting, runoff, and erosion response to soil water content and successive rainfalls. *Soil Sci. Soc. Am. J.* **56** (6), 1898–1903.

Chaplot, V. A. & Le Bissonnais, Y. 2003 Runoff features for interrill erosion at different rainfall intensities, slope lengths, and gradients in an agricultural loessial hillslope. *Soil Sci. Soc. Am. J.* **67** (3), 844–851.

Chen, H., Shao, M. & Li, Y. 2008 The characteristics of soil water cycle and water balance on steep grassland under natural and simulated rainfall conditions in the Loess Plateau of China. *J. Hydrol.* **360** (1), 242–251.

de Lima, J. L. & Abrantes, J. R. 2014 Using a thermal tracer to estimate overland and rill flow velocities. *Earth Surf. Processes Landforms* **39** (10), 1293–1300.

de Lima, R. L., Abrantes, J. R., de Lima, J. L. & Lima, M. I. P. 2015 Using thermal tracers to estimate flow velocities of shallow flows: laboratory and field experiments. *J. Hydrol. Hydromech.* **63** (3), 255–262.

Del Giudice, G., Padulano, R. & Rasulo, G. 2014 Spatial prediction of the runoff coefficient in Southern Peninsular Italy for the index flood estimation. *Hydrol. Res.* **45** (2), 263–281.

Dunkerley, D. 2001 Estimating the mean speed of laminar overland flow using dye injection-uncertainty on rough surfaces. *Earth Surf. Processes Landforms* **26** (4), 363–374.

Dunne, T., Zhang, W. & Aubry, B. F. 1991 Effects of rainfall, vegetation, and microtopography on infiltration and runoff. *Water Resour. Res.* **27** (9), 2271–2285.

Emmett, W. W. 1970 *The Hydraulics of Overland Flow on Hillslopes. 2330-7102*, US Government Printing Office.

Fang, H., Sun, L. & Tang, Z. 2015 Effects of rainfall and slope on runoff, soil erosion and rill development: an experimental study using two loess soils. *Hydrol. Processes* **29** (11), 2649–2658.

Fohrer, N., Berkenhagen, J., Hecker, J. M. & Rudolph, A. 1999 Changing soil and surface conditions during rainfall: single rainstorm/subsequent rainstorms. *Catena* **37** (3–4), 355–375.

Foster, G., Huggins, L. & Meyer, L. 1984 A laboratory study of rill hydraulics: I. Velocity relationships. *Trans. ASAE* **27** (3), 790–796.

Fox, D. M. & Bryan, R. B. 2000 The relationship of soil loss by interrill erosion to slope gradient. *Catena* **38** (3), 211–222.

Furumai, H., Jinadasa, H., Murakami, M., Nakajima, F. & Aryal, R. 2005 Model description of storage and infiltration functions of infiltration facilities for urban runoff analysis by a distributed model. *Water Sci. Technol.* **52** (5), 53–60.

Gardner, R. & Dunn, J. 1964 A single-sample radiotracer technique for determining stream flow rates. *Int. J. Appl. Radiation Isotopes* **15** (6), 339–344.

Horton, R. E., Leach, H. & Van Vliet, R. 1934 Laminar sheet-flow. *Eos, Trans. Am. Geophys. Union* **15** (2), 393–404.

King, K. & Norton, L. 1992 *Methods of Rill Flow Velocity Dynamics. Paper – American Society of Agricultural Engineers*. AGRIS, USA.

Lei, T., Chuo, R., Zhao, J., Shi, X. & Liu, L. 2010 An improved method for shallow water flow velocity measurement with practical electrolyte inputs. *J. Hydrol.* **390** (1), 45–56.

Li, G., Abrahams, A. D. & Atkinson, J. F. 1996 Correction factors in the determination of mean velocity of overland flow. *Earth Surf. Processes Landforms* **21** (6), 509–515.

Luk, S. & Merz, W. 1992 Use of the salt tracing technique to determine the velocity of overland flow. *Soil Technology* **5** (4), 289–301.

Meral, R. 2016 A study on the estimating of sediment concentration with turbidity and acoustic backscatter signal for different sediment sizes. *Hydrol. Res.* **47** (2), 305–311.

Muste, M., Hauet, A., Fujita, I., Legout, C. & Ho, H.-C. 2014 Capabilities of large-scale particle image velocimetry to characterize shallow free-surface flows. *Adv. Water Resour.* **70**, 160–171.

Nadal-Romero, E., Lasanta, T. & Garc-Ruiz, J. M. 2013 Runoff and sediment yield from land under various uses in a Mediterranean mountain area: long-term results from an experimental station. *Earth Surf. Processes Landforms* **38** (4), 346–355.

Philip, J. 1954 An infiltration equation with physical significance. *Soil Sci.* **77** (2), 153–158.

Planchon, O., Silvera, N., Gimenez, R., Favis-Mortlock, D., Wainwright, J., Bissonnais, Y. L. & Govers, G. 2005 An automated salt- tracing gauge for flow-velocity measurement. *Earth Surf. Processes Landforms* **30** (7), 833–844.

Rahma, A. E., Lei, T., Shi, X., Dong, Y., Zhou, S. & Zhao, J. 2013 Measuring flow velocity under straw mulch using the improved electrolyte tracer method. *J. Hydrol.* **495**, 121–125.

Schuetz, T., Weiler, M., Lange, J. & Stoelzle, M. 2012 Two-dimensional assessment of solute transport in shallow waters with thermal imaging and heated water. *Adv. Water Resour.* **43**, 67–75.

Shen, H., Zheng, F., Wen, L., Han, Y. & Hu, W. 2016 Impacts of rainfall intensity and slope gradient on rill erosion processes at loessial hillslope. *Soil Tillage Res.* **155**, 429–436.

Shi, Z., Ai, L., Li, X., Huang, X., Wu, G. & Liao, W. 2013 Partial least-squares regression for linking land-cover patterns to soil erosion and sediment yield in watersheds. *J. Hydrol.* **498**, 165–176.

Shi, Z., Huang, X., Ai, L., Fang, N. & Wu, G. 2014 Quantitative analysis of factors controlling sediment yield in mountainous watersheds. *Geomorphology* **226**, 193–201.

Singh, P., Ramasastri, K., Singh, U., Gergan, J. & Dobhal, D. 1995 Hydrological characteristics of the Dokriani Glacier in the Garhwal Himalayas. *Hydrol. Sci. J.* **40** (2), 243–257.

Singh, P., Haritashya, U. K., Ramasastri, K. & Kumar, N. 2005 Diurnal variations in discharge and suspended sediment concentration, including runoff-delaying characteristics, of the Gangotri Glacier in the Garhwal Himalayas. *Hydrol. Processes* **19** (7), 1445–1457.

Sun, W., Yao, X., Cao, N., Xu, Z. & Yu, J. 2016 Integration of soil hydraulic characteristics derived from pedotransfer functions into hydrological models: evaluation of its effects on simulation uncertainty. *Hydrol. Res.* **47** (5), 964–978.

Tauro, F., Grimaldi, S., Petroselli, A. & Porfiri, M. 2012a Fluorescent particle tracers for surface flow measurements. *Water Resour. Res.* **48** (6), W06528.

Tauro, F., Grimaldi, S., Petroselli, A., Rulli, M. & Porfiri, M. 2012b Fluorescent particle tracers in surface hydrology: a proof of concept in a semi-natural hillslope. *Hydrol. Earth Syst. Sci.* **16** (8), 2973–2983.

Ventura, E., Nearing, M. A. & Norton, L. D. 2001 Developing a magnetic tracer to study soil erosion. *Catena* **43** (4), 277–291.

Williams, J. & Berndt, H. 1977 Sediment yield prediction based on watershed hydrology. *Trans. ASAE* **20** (6), 1100–1104.

Wilson, L. 1973 Variations in mean annual sediment yield as a function of mean annual precipitation. *Am. J. Sci.* **273** (4), 335–349.

Xia, W., Liu, C., Lei, T., Hu, Y. & Zhao, J. 2007 Analysis of faults in theory for measuring flow velocity on slope with tracer method. *J. Natural Disasters* **16** (1), 50–54 (in Chinese with English abstract).

Yan, B., Fang, N., Zhang, P. & Shi, Z. 2013 Impacts of land use change on watershed streamflow and sediment yield: an assessment using hydrologic modelling and partial least squares regression. *J. Hydrol.* **484**, 26–37.

Zhang, G., Liu, B., Liu, G., He, X. & Nearing, M. 2003 Detachment of undisturbed soil by shallow flow. *Soil Sci. Soc. Am. J.* **67** (3), 713–719.

Zhang, G., Luo, R., Cao, Y., Shen, R. & Zhang, X. 2010 Correction factor to dye-measured flow velocity under varying water and sediment discharges. *J. Hydrol.* **389** (1), 205–213.

Zhang, G., Liu, G., Yi, L. & Zhang, P. 2014 Effects of patterned Artemisia capillaris on overland flow resistance under varied rainfall intensities in the Loess Plateau of China. *J. Hydrol. Hydromech.* **62** (4), 334–342.

Zhang, W., Yuan, J., Han, J., Huang, C. & Li, M. 2016 Impact of the Three Gorges Dam on sediment deposition and erosion in the middle Yangtze River: a case study of the Shashi Reach. *Hydrol. Res.* **47** (S1), 175–186.

First received 5 March 2017; accepted in revised form 26 July 2017. Available online 4 October 2017